UNSEEN trends: Detecting decadal changes in 100-year precipitation extremes

T. Kelder[1,2]*, M. Müller[2,3], L.J. Slater[4], T.I. Marjoribanks[5], R.L. Wilby[1], C. Prudhomme[6,7], P. Bohlinger[2], L. Ferranti[6], T. Nipen[2]

[1]Geography and Environment, Loughborough University, Loughborough, UK

[2]The Norwegian Meteorological Institute, Oslo, Norway

[3]Section for Meteorology and Oceanography, Department of Geosciences, University of Oslo, Norway

[4]School of Geography and the Environment, University of Oxford, Oxford, UK

[5]School of Architecture, Building and Civil Engineering, Loughborough, UK

[6]European Centre for Medium-Range Weather Forecasts (ECMWF), Reading, UK

[7]Centre for Ecology and Hydrology, Wallingford, UK

* T.Kelder@lboro.ac.uk

This is a preprint of an article published in Npj Climate and Atmospheric Science. The final authenticated version is available online at: https://doi.org/10.1038/s41612-020-00149-4.

Sample sizes of observed climate extremes are typically too small to reliably constrain non-stationary behaviour. To facilitate detection of non-stationarities in 100-year precipitation values over a short period of 35 years (1981-2015), we apply the UNprecedented Simulated Extreme ENsemble (UNSEEN) approach, by pooling ensemble members and lead times from the ECMWF seasonal prediction system SEAS5. We generate a 3500-year UNSEEN dataset of autumn 3-day extreme precipitation events across Western Norway and Svalbard. The UNSEEN ensemble shows that an event of 1.5 times the magnitude of the most severe flood episode recorded in Western Norway can arise with a return period of ~2000 years. Applying the novel UNSEEN-trends approach, we demonstrate that for Svalbard the 100-year event in 1981 could be expected to occur with a return period of around 40 years in 2015. These new insights have important implications for current design-level practices and for understanding the underlying causes of non-stationarities.

Handling the non-stationarity of climate extremes is an active area of research[1–3] that is confounded by the brevity and sparsity of observational records[4–6]. Non-stationary precipitation analyses typically focus on detecting multidecadal to centennial changes in annual precipitation maxima[7–9].

However, annual maximum precipitation events do not necessarily cause high impacts and hence, a potentially more pressing research challenge is the detection of changes in larger extremes[10,11], such as the 1-in-100-year event. Furthermore, the impacts of abrupt warming in recent decades may not yet be detectable in short precipitation records. Therefore, robust detection of short-term (decadal, rather than centennial) trends in climate extremes may provide valuable and actionable information.

An emerging alternative to traditional observation-based extreme value analysis is to pool ensemble members from numerical weather prediction systems[12–22] – the UNprecedented Simulated Extreme ENsemble (UNSEEN) approach[20,22]. This technique creates numerous alternative pathways of reality, thus increasing the event sample size for statistical analysis. The larger sample size offers a broader view of present-day hazard and, therefore, has potential to improve design-levels. For example, the 2013/14 winter flooding in the UK had no observational precedent, but could have been anticipated with the UNSEEN approach[22]. Similarly, estimates of storm surge levels of the River Rhine[12,13], global ocean wind and wave extremes[15,16,18], and losses from extreme windstorms[19] have all been improved with the UNSEEN approach. UNSEEN can also enhance food security through better drought exposure estimates[14,21] and can assist policy makers and contingency planners by quantifying and explaining the most severe events possible in the current climate, such as heatwaves in China[20]. However, validating the UNSEEN method is a well-recognised difficulty in existing studies, and UNSEEN has not yet been used to facilitate detection of non-stationarity in climate extremes over short periods of several decades.

Here, we provide a framework to systematically evaluate the robustness of the UNSEEN approach and we present a novel UNSEEN-trends approach, where we aim to provide confident short-term trend estimates by using the larger event sample to better constrain changes in climate extremes. We do this in a storyline context[23], where we take observed flood episodes as a starting point for our analysis. We select the west coast of Norway and the Svalbard Archipelago as study regions; two contrasting areas in terms of precipitation extremes. Western Norway faces the highest extremes within Europe[24] and has a dense station network[25,26], whereas Svalbard is a semi-desert with only a few observation stations[27]. Both regions have faced severe damages from recent extreme events, such as the September 2005[28] and October 2014[29] floods over Western Norway and the slush-avalanche inducing extreme precipitation event over the Svalbard Archipelago in 2012[30]. The extreme events were driven by atmospheric rivers[27–29] (ARs), which cause heavy precipitation over a prolonged period. As AR-related floods predominantly occur in autumn and frequently strengthen over a period of several days[28,29], we select autumn (September to November) spatial averaged (Supplementary fig. 1) three-day extreme precipitation (SON-3DP) as target events.

Previous UNSEEN studies have used the Hadley Centre global climate model, HadGEM3-GC2[14,20–22] and the European Centre for Medium-ranged Weather Forecasts (ECMWF) ensemble prediction systems[15–18] and earlier version of the seasonal prediction system[12,13,19]. Here, we are the first to use the latest ECMWF seasonal prediction system SEAS5[31] for its high-resolution, large ensemble, long homogeneous hindcast period (1981-2015) and open access. The ECMWF atmospheric model has shown skill in simulating atmospheric rivers for Northern Europe[32], giving confidence in the realism of these extreme events in SEAS5, hence is a good candidate for the UNSEEN method. We use the 25 ensemble members across lead times of 2-5 months, resulting in a sample of 100 members (called the UNSEEN ensemble) and evaluate the independence and stability of the pooled sample for SON-3DP events across Western Norway and Svalbard. We then use the UNSEEN-trends approach to identify unprecedented extreme precipitation events and to detect trends in 100-year precipitation events over the last 35 years. These findings will help understanding the robustness of current design levels and may improve our understanding of physical processes driving climate extremes and their non-stationarity.

Ensemble member independence and model stability

The independence of ensemble members is an important requirement for the UNSEEN approach, as dependent members would artificially inflate the sample size, without adding new information. Previous studies have assessed the independence of ensemble members for lead times 9-10 days[15,16,18], but to the best of our knowledge, no independence test has yet been performed in UNSEEN studies of seasonal prediction systems.

For the regions studied here, the ensemble members from lead times beyond one month are not dependent on atmospheric initial conditions, because the synoptic patterns related to ARs are known not to be predictable beyond two weeks[32,33]. However, predictability on a seasonal timescale may be found through slowly varying components of the ocean-atmosphere system. Therefore, while the ensemble members might represent unique weather events because of the independency to the atmospheric initial conditions, the weather events could have a conditional bias induced by favourable conditions in the slowly varying components of the ocean-atmosphere system.

To test the seasonal dependence of SON-3DP, we first select the seasonal maximum event for each forecast then concatenating these events to create a 35-year timeseries (Fig. 1a,b,c). To robustly assess the independence between each of the ensemble members, we calculate the Spearman rank correlation coefficient (ρ) for every distinct pair of ensemble members (Fig. 1d), resulting in 300 ρ values for each lead time. The value of ρ ranges from ca. −0.6 to 0.6, and the median correlation is close to zero for all lead times for both Western Norway and Svalbard (Fig. 1e,f). The range in ρ

values is expected due to the large number of correlation tests, and none of the lead times fall outside the range that would be expected for uncorrelated data for the West Coast of Norway (Fig. 1e). For Svalbard, slightly higher ρ values are found, with the median correlation still within the expected range, but the interquartile range just exceeding the upper boundary of the confidence intervals for the first two lead times (Fig. 1f). The small correlations found for Svalbard might be driven by the trend that we detect for this region (UNSEEN-trends section), and thus, the UNSEEN ensemble members represent unique events that follow the slowly evolving climate signal, as desired.

A second potential issue for generating the UNSEEN ensemble could be a drift in the simulated climatology[34,35], which may alter precipitation extremes over longer lead times. Therefore, model stability is a requirement for pooling lead times. Model stability is assessed by comparing the distribution of predicted SON-3DP events across different lead times. For both regions, the probability density functions of the pooled SON-3DP events for the considered lead times are remarkably similar (Fig. 2a,b). Moreover, the empirical extreme value distributions of the individual lead times fall within the uncertainty range of the distribution of all lead times pooled together and thus, the model can be considered stable over lead times (Fig. 2c,d).

Fidelity of UNSEEN extremes for Western Norway

Confidence in simulated `unprecedented extremes' in large ensembles is complicated by the inability to validate extremes, given the limited sample sizes of observations. Here, we evaluate the UNSEEN ensemble with 1) rank histograms, commonly applied in ensemble forecast verification[36] and 2) by bootstrapping the ensemble into datasets of 35 years and assessing whether observations fall within the range of the bootstrapped distribution, following previous UNSEEN studies[20,22] (see Methods). We perform this analysis for the SEAS5 UNSEEN SON-3DP ensemble over Western Norway, because the dense station network of the country[25,26] facilitates model evaluation (unlike in Svalbard). For a comprehensive global model validation of SEAS5, see Johnson *et al.*[31].

The rank histograms clearly indicate an under-forecasting bias of the absolute SON-3DP values within the UNSEEN ensemble (Supplementary Fig. 2). This is confirmed by the bootstrapping test, that shows that the observed mean and standard deviation fall outside the 95% confidence intervals of the UNSEEN ensemble (Supplementary Fig. 3). The UNSEEN SON-3DP anomalies and standardized anomalies do show rank uniformity, and thus are suggested to be reliable (Supplementary Fig. 2). Such under-forecasting biases precipitation extremes are not uncommon in global Earth System Models[37], especially for a mountainous region like Western Norway.

As the UNSEEN SON-3DP deviations from the mean show good agreement to the observed values (Supplementary Fig. 2), the ratio between the mean observed extremes and the mean simulated extremes (1.74) is applied as a constant bias correction to generate the bias corrected UNSEEN ensemble (henceforth referred to as UNSEEN-BC). Note that we found little sensitivity to using the median (1.72), 5-year (1.69) or 20-year (1.70) values in the bias correction procedure and, hence chose a constant value to avoid extrapolations beyond the quantile range. The bootstrapping test shows that the statistics derived from the observed precipitation fall within the 95% intervals of UNSEEN-BC for timeseries of 35 years (Supplementary Fig. 4), i.e. the precipitation of the single realization of reality is one of the plausible realizations of UNSEEN-BC and, therefore, UNSEEN-BC is indistinguishable from the observed values.

We then fit the GEV distribution to the observations, the UNSEEN and the UNSEEN-BC ensemble (see Methods and Fig. 3). Interestingly, the fitted distributions show that the UNSEEN-BC ensemble diverges from the observed values for return periods above ~35 years. To evaluate the discrepancy, we test the sensitivity of the results to the choice of extreme value distribution (Supplementary Fig. 5). Whilst the Gumbel distribution (shape parameter $\xi = 0$) shows a relatively good fit to the observations and a similar distribution to the UNSEEN ensemble, the fit is not as good as using a full GEV with fitted shape parameter, as suggested by Supplementary Fig. 5 and confirmed by the likelihood ratio test (p-value = 0.03 for the observed and p-value = $1.54 * 10^{-7}$ for the UNSEEN ensemble). In addition, results are also very sensitive to outliers, as can be seen when the observed extreme value distribution is fitted on a sample where the largest value is increased by 10% (Supplementary Fig. 5). This confirms the challenge associated with estimating the magnitude of events of long return periods (greater than 20 years) from an observed time series of only 35 years, with more trust in estimations resulting from the larger UNSEEN sample.

We find that the 2005 and 2014 observed extreme events (two largest events in Fig. 3) are similar in magnitude and represent events with return periods of 21 years (CI of 19-24 years) when compared with the extreme value distribution of UNSEEN-BC. Based on the observed values, the return period estimate of 60 years for the events would be very uncertain, with the lower confidence interval never reaching the event magnitude (CI of 18 - ∞ years). Moreover, the highest UNSEEN-BC event is 1.5 times higher than the highest observed event, with an estimated return period of ~2000 years (CI of 1150-4800 years). The estimated return period of this event based on the observations is completely dominated by the uncertainties (~5000, 600 - ∞ years) and can only be statistically modelled, while for the UNSEEN estimate, it is a physically simulated `empirical' event within 3500 years of data. The observed flood episode caused flooding and landslides with severe damage[28] and

UNSEEN-BC indicates what kind of events beyond the observed record are plausible in the present climate.

UNSEEN-trends in 100-year precipitation over last 35 years

Climate models can be used to detect changes[38–41] or to attribute extreme events to human causes[42], but are less suited to detecting trends over the recent past such as the last 35 years. By design, climate model simulations are initialized once at the beginning of a centennial run. Contrastingly, here we use seasonal forecasts that are initialized every month, and thus are more constrained by real-world climate variability than climate model simulations. Consequently, seasonal forecasts sample a smaller range of climate conditions but are closer to reality than climate model simulations. This means that their use is consistent with analysing trends over the recent past described by the available forecast period (for SEAS5, currently 35 years). Furthermore, the model setup and version are the same for the entire hindcast simulation, ensuring that, with respect to the models and initialization, SEAS5 is a homogeneous dataset and thus suitable for climate analysis and detection of UNSEEN-trends.

With a 36 km resolution and 25 members, the ECMWF SEAS5 reforecast set used here is based on a modelling system of high resolution and associated with a large ensemble compared to current high-resolution global climate models[43]. SEAS5 greenhouse gas radiative forcing captures the long-term trends in emissions[31], and we show that the global mean temperature trend in SEAS5 follows ERA5[44] (Supplementary Fig.6). Whilst regionally, we find a cold bias over the Norwegian study domain, the trend is consistent with ERA5 for both Western Norway and Svalbard (Supplementary Fig. 6), confirming the capacity of SEAS5 to detect recent trends.

To illustrate the added value of UNSEEN-trends, we extend the GEV distribution to include a time covariate and fit this distribution to the observed and UNSEEN SON-3DP (see Methods). Using the observations, we find an increase in 100-year SON-3DP of 4% over 1981-2015 in Western Norway, but associated with large uncertainties ranging from −27% to 34% (Fig. 4 a,b). The UNSEEN-trend estimate of 2% is more constrained due the larger sample size, with confidence intervals ranging from −3% to 7%. A negative trend is thus statistically possible, indicating that the trend over Western Norway is not significant. For Svalbard, we find a significant positive UNSEEN-trend of 8%, with uncertainty bounds ranging between 4-12%.

In addition to the trend in 100-year SON-3DP events, we illustrate the change in all return values by plotting the GEV distribution with the covariates 1981 and 2015 (Fig. 4 c,d). The likelihood ratio test shows that the GEV distribution including a time covariate improves the model fit for Svalbard (p-value = 2.7e-07). We find that the frequency of the event that used to be a 100-year event in 1981 has an expected return period of 41 years in 2015 (Fig. 4 c,d). For Western Norway, the GEV distribution including a time covariate does not improve the model fit for either the observed (p-value = 0.58) or the UNSEEN-ensemble (p-value = 0.65), and thus, the stationary GEV distribution, as presented in Fig. 3, is most appropriate.

Discussion and Conclusion

In this study, we test the robustness of the UNSEEN approach and we use the large sample to constrain short-term UNSEEN-trends in high-impact precipitation events for Western Norway and Svalbard. We show that with SEAS5, the effective sample size of autumn 3-day precipitation (SON-3DP) events in Western Norway and Svalbard can be increased by a factor of 100 compared to observations, because ensemble members are independent and the model is stable over lead times. Validating UNSEEN events and trends is a complex task, but our approach reproduces observed extremes well after bias correction for Western Norway, a region with extensive records[26].

The insights presented in this study are specific to Western Norway and Svalbard SON-3DP but the independence, model stability and model fidelity tests applied to the UNSEEN approach could be transferred to other regions, temporal resolutions and spatial extent of the events, seasons and climate variables. Global validation of the UNSEEN ensemble will highlight in which regions the approach may enhance the robustness of design level estimation, with a potentially high value in supporting data scarce regions[45]. Furthermore, the large sample size may allow estimation of extremes using empirical approaches that avoid assumptions about underlying distributions and their non-stationarity, thereby offering the possibility of improved design estimates[10] and empirical attribution of physical mechanisms. A wide range of scientific disciplines might benefit from the UNSEEN method by forcing seasonal prediction systems into impact models to assess unprecedented impacts and improve understanding of the physical mechanisms leading to these events.

The results from the two study areas highlight the value of both the UNSEEN and the UNSEEN-trends approach. For the well-monitored Norwegian domain, we are able to bias correct the UNSEEN ensemble (UNSEEN-BC) and therefore we can better estimate the return period of the 2005 and 2014 flood episodes. We find that the flood episodes are not rare exceptions; rather they might be expected to occur once in 20 years under a stationary climate. Furthermore, the UNSEEN-BC ensemble shows that an event of 1.5 times the magnitude of the highest observed event could arise. The September 2005 and October 2014 flood episodes were identified as high-impact events in previous end-user engagement sessions within the Translating Weather Extremes into the Future

(TWEX) project, and thus, the results found from the UNSEEN-BC ensemble are of high relevance to decision makers and end-users. This application of the UNSEEN approach is similar to previous research on the 2013/14 winter floods in the UK[22] and for the 1990 windstorm losses over Germany and the UK[19]. A difference to the previous studies is that we run the analysis on a three-day resolution, whereas monthly averages have been used so far. The observed record and the UNSEEN-trend show that there is no significant trend over Western Norway between 1981-2015, and therefore justify using the stationary GEV distribution.

Contrastingly, for Svalbard, the UNSEEN-trends approach shows that what was a 100-year event in 1981 is to be expected to return once in 41 years in 2015. The trend in extreme precipitation over Svalbard could not be detected from observation-based studies due to the sparse observation network in this area[27]. Despite very few precipitation extremes being recorded in the Svalbard Archipelago, it is assumed that their frequency and magnitude are increasing in a warming climate[27,30,46], which is confirmed by our UNSEEN-trends analysis. Those precipitation extremes are connected to the inflow of relatively warm air and, thus, can cause severe landslides and so-called rain-on-ice events[30]. Both could have significant impacts on people living in the Arctic and on the local ecosystem.

In due course, the drivers of changes in climate extremes could be investigated with the UNSEEN-trends approach. For example, to assess the non-stationarity of extreme precipitation, covariates other than time could be selected, such as ocean temperatures, modes of climate variability, or indicators of large-scale synoptic weather systems. This may improve our physical understanding of the non-stationary processes and could provide insight into potential model biases, thereby improving confidence in detected trends. Century-long seasonal hindcasts, such as the ASF-20C global atmospheric seasonal hindcasts[47], might prove useful in assessing the sensitivity of UNSEEN-trends to different time windows over a longer time period.

Our results for Western Norway highlight the strength of UNSEEN in estimating design-levels and present-day climate hazards, backed by a growing body of literature[12,13,22,14–21], and the results for Svalbard emphasise the significance of our novel UNSEEN-trends approach in estimating non-stationarities in climate extremes. Both underline the need to rethink current design-level estimates based upon observations alone. We think further applications can 1) help estimate design values, especially relevant for data scarce regions; 2) improve risk estimation of natural hazards by coupling UNSEEN to impact models; 3) detect trends in rare climate extremes, including variables other than precipitation; and 4) increase our physical understanding of the drivers of non-stationary climate extremes, through the possible attribution of detected trends.

References

1. IPCC. Summary for Policymakers. in *Global Warming of 1.5°C. An IPCC Special Report on the impacts of global warming of 1.5°C above pre-industrial levels and related global greenhouse gas emission pathways, in the context of strengthening the global response to the threat of climate change,* 32 (World Meteorological Organization, 2018).

2. IPCC. Summary for Policymakers. in *Managing the Risks of Extreme Events and Disasters to Advance Climate Change Adaptation: Special Report of the Intergovernmental Panel on Climate Change* 3–22 (Cambridge University Press, 2012). doi:10.1017/CBO9781139177245.003.

3. IPCC. Summary for Policymakers. in *Climate Change 2014: Impacts, Adaptation, and Vulnerability. Part A: Global and Sectoral Aspects. Contribution of Working Group II to the Fifth Assessment Report of the Intergovernmental Panel on Climate Change* 1–32 (Cambridge University Press, 2014). doi:10.1017/CBO9781107415379.003.

4. Wilby, R. L. *et al.* The 'dirty dozen'of freshwater science: detecting then reconciling hydrological data biases and errors. *Wiley Interdiscip. Rev. Water* **4**, e1209 (2017).

5. Zwiers, F. W. *et al.* Climate Extremes: Challenges in Estimating and Understanding Recent Changes in the Frequency and Intensity of Extreme Climate and Weather Events. in *Climate Science for Serving Society* 339–389 (Springer Netherlands, 2013). doi:10.1007/978-94-007-6692-1_13.

6. Alexander, L. V. Global observed long-term changes in temperature and precipitation extremes: a review of progress and limitations in IPCC assessments and beyond. *Weather Clim. Extrem.* **11**, 4–16 (2016).

7. Klein Tank, A. M. G. & Können, G. P. Trends in Indices of Daily Temperature and Precipitation Extremes in Europe, 1946–99. *J. Clim.* **16**, 3665–3680 (2003).

8. Westra, S., Alexander, L. V & Zwiers, F. W. Global increasing trends in annual maximum daily precipitation. *J. Clim.* **26**, 3904–3918 (2013).

9. Donat, M. G., Lowry, A. L., Alexander, L. V, O'Gorman, P. A. & Maher, N. More extreme precipitation in the world's dry and wet regions. *Nat. Clim. Chang.* **6**, 508 (2016).

10. der Wiel, K., Wanders, N., Selten, F. M. & Bierkens, M. F. P. Added Value of Large Ensemble Simulations for Assessing Extreme River Discharge in a 2 °C Warmer World. *Geophys. Res. Lett.* **46**, (2019).

11. Berghuijs, W. R., Aalbers, E. E., Larsen, J. R., Trancoso, R. & Woods, R. A. Recent changes in extreme floods across multiple continents. *Environ. Res. Lett.* **12**, 114035 (2017).

12. van den Brink, H. W., Können, G. P., Opsteegh, J. D., van Oldenborgh, G. J. & Burgers, G. Improving 10^{4}-year surge level estimates using data of the ECMWF seasonal prediction system. *Geophys. Res. Lett.* **31**, L17210 (2004).

13. van den Brink, H. W., Können, G. P., Opsteegh, J. D., van Oldenborgh, G. J. & Burgers, G. Estimating return periods of extreme events from ECMWF seasonal forecast ensembles. *Int. J. Climatol.* **25**, 1345–1354 (2005).

14. Kent, C. *et al.* Maize Drought Hazard in the Northeast Farming Region of China: Unprecedented Events in the Current Climate. *J. Appl. Meteorol. Climatol.* **58**, 2247–2258

(2019).

15. Breivik, Ø., Aarnes, O. J., Abadalla, S., Bidlot, J.-R. & Janssen, P. Wind and Wave Extremes over the World Oceans From Very Large Ensembles. *Geophys. Res. Lett.* **41**, 5122–5131 (2014).

16. Breivik, Ø., Aarnes, O. J., Bidlot, J.-R., Carrasco, A. & Saetra, Ø. Wave Extremes in the Northeast Atlantic from Ensemble Forecasts. *J. Clim.* **26**, 7525–7540 (2013).

17. Osinski, R. *et al.* An approach to build an event set of European windstorms based on ECMWF EPS. *Nat. Hazards Earth Syst. Sci.* **16**, 255–268 (2016).

18. Meucci, A., Young, I. R. & Breivik, Ø. Wind and Wave Extremes from Atmosphere and Wave Model Ensembles. *J. Clim.* **31**, 8819–8842 (2018).

19. Walz, M. A. & Leckebusch, G. C. Loss potentials based on an ensemble forecast: How likely are winter windstorm losses similar to 1990? *Atmos. Sci. Lett.* **20**, e891 (2019).

20. Thompson, V. *et al.* Risk and dynamics of unprecedented hot months in South East China. *Clim. Dyn.* **52**, 2585–2596 (2019).

21. Kent, C. *et al.* Using climate model simulations to assess the current climate risk to maize production. *Environ. Res. Lett.* **12**, (2017).

22. Thompson, V. *et al.* High risk of unprecedented UK rainfall in the current climate. *Nat. Commun.* **8**, 107 (2017).

23. Shepherd, T. G. *et al.* Storylines: an alternative approach to representing uncertainty in physical aspects of climate change. *Clim. Change* **151**, 555–571 (2018).

24. Lavers, D. A. & Villarini, G. The contribution of atmospheric rivers to precipitation in Europe and the United States. *J. Hydrol.* **522**, 382–390 (2015).

25. Lussana, C. *et al.* seNorge2 daily precipitation, an observational gridded dataset over Norway from 1957 to the present day. *Earth Syst. Sci. Data* **10**, 235–249 (2018).

26. Lussana, C., Tveito, O. E., Dobler, A. & Tunheim, K. seNorge_2018, daily precipitation and temperature datasets over Norway. *Earth Syst. Sci. Data Discuss.* **2019**, 1–27 (2019).

27. Serreze, M. C., Crawford, A. D. & Barrett, A. P. Extreme daily precipitation events at Spitsbergen, an Arctic Island. *Int. J. Climatol.* **35**, 4574–4588 (2015).

28. Stohl, A., Forster, C. & Sodemann, H. Remote sources of water vapor forming precipitation on the Norwegian west coast at 60°N - A tale of hurricanes and an atmospheric river. *J. Geophys. Res. Atmos.* **113**, (2008).

29. Langsholt, E., Roald, L. A., Holmqvist, E. & Fleig, A. *Flommen på Vestlandet oktober 2014*. *NVE Report* www.nve.no (2015).

30. Hansen, B. B. *et al.* Warmer and wetter winters: characteristics and implications of an extreme weather event in the High Arctic. *Environ. Res. Lett.* **9**, 114021 (2014).

31. Johnson, S. J. *et al.* SEAS5: The new ECMWF seasonal forecast system. *Geosci. Model Dev. Discuss.* (2018) doi:https://doi.org/10.5194/gmd-12-1087-2019.

32. Lavers, D. A., Pappenberger, F. & Zsoter, E. Extending medium-range predictability of extreme hydrological events in Europe. *Nat. Commun.* **5**, 5382 (2014).

33. Baggett, C. F., Barnes, E. A., Maloney, E. D. & Mundhenk, B. D. Advancing atmospheric river forecasts into subseasonal-to-seasonal time scales. *Geophys. Res. Lett.* **44**, 7528–7536 (2017).

34. Gupta, A. Sen, Jourdain, N. C., Brown, J. N. & Monselesan, D. Climate drift in the CMIP5 models. *J. Clim.* **26**, 8597–8615 (2013).

35. Hermanson, L. *et al.* Different types of drifts in two seasonal forecast systems and their dependence on ENSO. *Clim. Dyn.* **51**, 1411–1426 (2018).

36. Wilks, D. S. *Statistical methods in the atmospheric sciences*. vol. 100 (Academic press, 2011).

37. Sillmann, J., Kharin, V. V., Zhang, X., Zwiers, F. W. & Bronaugh, D. Climate extremes indices in the CMIP5 multimodel ensemble: Part 1. Model evaluation in the present climate. *J. Geophys. Res. Atmos.* **118**, 1716–1733 (2013).

38. Kharin, V. V *et al.* Risks from climate extremes change differently from 1.5 °C to 2.0 °C depending on rarity. *Earth's Futur.* (2018) doi:https://doi.org/10.1002/2018EF000813.

39. Kharin, V. V, Zwiers, F. W., Zhang, X. & Wehner, M. Changes in temperature and precipitation extremes in the CMIP5 ensemble. *Clim. Change* **119**, 345–357 (2013).

40. Sillmann, J., Kharin, V. V, Zwiers, F. W., Zhang, X. & Bronaugh, D. Climate extremes indices in the CMIP5 multimodel ensemble: Part 2. Future climate projections. *J. Geophys. Res. Atmos.* **118**, 2473–2493 (2013).

41. Kharin, V. V & Zwiers, F. W. Changes in the extremes in an ensemble of transient climate simulations with a coupled atmosphere--ocean GCM. *J. Clim.* **13**, 3760–3788 (2000).

42. Angélil, O. *et al.* Comparing regional precipitation and temperature extremes in climate model and reanalysis products. *Weather Clim. Extrem.* **13**, 35–43 (2016).

43. Haarsma, R. J. *et al.* High Resolution Model Intercomparison Project (HighResMIP v1.0) for CMIP6. *Geosci. Model Dev.* **9**, 4185–4208 (2016).

44. Hersbach, H. *et al. Operational global reanalysis: progress, future directions and synergies with NWP including updates on the ERA5 production status*. *ERA Report Series No. 27* (2018) doi:10.21957/tkic6g3wm.

45. Courty, L. G., Wilby, R. L., Hillier, J. K. & Slater, L. J. Intensity-duration-frequency curves at the global scale. *Environ. Res. Lett.* **14**, (2019).

46. Hanssen-Bauer, I. *et al. Climate in Svalbard 2100*. (2019).

47. Weisheimer, A., Schaller, N., O'Reilly, C., MacLeod, D. A. & Palmer, T. Atmospheric seasonal forecasts of the twentieth century: multi-decadal variability in predictive skill of the winter North Atlantic Oscillation (NAO) and their potential value for extreme event attribution. *Q. J. R. Meteorol. Soc.* **143**, 917–926 (2017).

48. Madec, G. & others. NEMO ocean engine. *Note du Pôle modélisation l'Institut Pierre-Simon Laplace No 27* ISSN No 1288-1619 (2016).

49. Fichefet, T. & Maqueda, M. A. Sensitivity of a global sea ice model to the treatment of ice thermodynamics and dynamics. *J. Geophys. Res. Ocean.* **102**, 12609–12646 (1997).

50. Dee, D. P. *et al.* The ERA-Interim reanalysis: Configuration and performance of the data assimilation system. *Q. J. R. Meteorol. Soc.* **137**, 553–597 (2011).

51. Zuo, H., Alonso-Balmaseda, M. A., Mogensen, K. & Tietsche, S. OCEAN5: The ECMWF Ocean Reanalysis System and its Real-Time analysis component. *ECMWF Tech. Memo.* (2018) doi:https://doi.org/10.21957/la2v0442.

52. Azad, R. & Sorteberg, A. Extreme daily precipitation in coastal western Norway and the link to

atmospheric rivers. *J. Geophys. Res. Atmos.* **122**, 2080–2095 (2017).

53. Benedict, I., Ødemark, K., Nipen, T. & Moore, R. Large-scale flow patterns associated with extreme precipitation and atmospheric rivers over Norway. *Mon. Weather Rev.* **147**, 1415–1428 (2019).

54. Zhang, X. *et al.* Indices for monitoring changes in extremes based on daily temperature and precipitation data. *Wiley Interdiscip. Rev. Clim. Chang.* **2**, 851–870 (2011).

55. Hoyer, S. & Hamman, J. J. xarray: N-D labeled Arrays and Datasets in Python. *J. Open Res. Softw.* **5**, (2017).

56. Gómez-Rubio, V. ggplot2 - Elegant Graphics for Data Analysis (2nd Edition). *J. Stat. Softw.* **77**, (2017).

57. Press, S. J. *Applied multivariate analysis: using Bayesian and frequentist methods of inference*. (Courier Corporation, 2005).

58. R Core Team. R: A Language and Environment for Statistical Computing. https://www.R-project.org (2019).

59. Hyndman, R. J. & Fan, Y. Sample Quantiles in Statistical Packages. *Am. Stat.* **50**, 361–365 (1996).

60. Coles, S., Bawa, J., Trenner, L. & Dorazio, P. *An introduction to statistical modeling of extreme values*. vol. 208 (Springer, 2001).

61. Gilleland, E., Katz, R. W. & others. extRemes 2.0: an extreme value analysis package in R. *J. Stat. Softw.* **72**, 1–39 (2016).

62. Katz, R. W., Parlange, M. B. & Naveau, P. Statistics of extremes in hydrology. *Adv. Water Resour.* **25**, 1287–1304 (2002).

63. Katz, R. W. Statistical methods for nonstationary extremes. in *Extremes in a Changing Climate* 15–37 (Springer, 2013).

64. Rojas, R., Feyen, L. & Watkiss, P. Climate change and river floods in the European Union: Socio-economic consequences and the costs and benefits of adaptation. *Glob. Environ. Chang.* **23**, 1737–1751 (2013).

Methods

Data. We use the fifth generation of the ECMWF seasonal forecasting system SEAS5 to generate the UNSEEN ensemble. SEAS5 is a global coupled ocean, sea-ice, and atmosphere model, which has been introduced in fall 2017[31]. The atmospheric component is based on cycle 43r1 of the ECMWF Integrated Forecast System. The spatial horizontal resolution is 36 km and it has 91 vertical levels. The ocean (Nucleus for European Modelling of the Ocean, NEMO[48]) and sea-ice (Louvain-la-Neuve Sea Ice Model, LIM2[49]) models run on a 0.25-degree resolution. The atmosphere is initialized by ERA-Interim[50] and the ocean and sea-ice components are initialized by the OCEAN5 reanalysis[51]. ECMWF provides a re-forecast (also known as hindcast) dataset for calibration of the operational forecasting system SEAS5. The data are initialized monthly with 25 ensemble members, each with 7-month forecast length on a daily resolution, covering the years 1981-2016[31]. The ensemble members are generated from perturbations to the ocean and atmosphere initial conditions and from stochastic model perturbations.

In the UNSEEN approach, ensemble members and initialization dates are pooled to increase the sample size of the variable of interest. Here, we generate an UNSEEN ensemble for the west coast of Norway and for the Svalbard Archipelago to focus on recent atmospheric river (AR) related severe events[27–29]. ARs have been connected to precipitation extremes in the observed records for both Norway[52,53] and Svalbard[27] and occur in September to March. AR-related floods mostly occur in autumn, because snowfall during winter precipitation events results in storage rather than runoff. One-day and five-day precipitation are a common diagnostic for extreme analysis[6,54]. ARs frequently strengthen over a period of several days[28,29] and therefore multi-day diagnostics prevent splitting events. Following the 2014 flood episode[29], we have chosen three-day total precipitation in this study. We thus select autumn (September to November) 3-day extreme precipitation (SON-3DP) as target events.

Since the forecasts are initialized every month on the first of the month and run over 7-months length, there are five initialization months (May-September) available to forecast the entire target autumn season (September-November). The first month is removed to avoid potentially dependent events. In the end, 100 forecasts, based on 25 ensemble members with 4 initialization dates are used to forecast the autumn season of each year (Fig. 1a-c). The window of 35 years between 1981 and 2016 leads to a total of 3500 forecasts of autumn weather conditions that could have occurred. We extract the maximum 3-day cumulative precipitation within autumn from the 3500 forecasts (SON-3DP), using the xarray package[55] in Python. To focus on the large-scale systems as experienced in recent severe events, we use only the large-scale precipitation output of the model. The west coast of Norway is mountainous and characterised by large topographic variations. Catchment-scale processes in these mountainous areas cannot be resolved by a global model with 36 km resolution. Therefore, the precipitation timeseries presented in this study are spatial averages where the 200-year precipitation exceeds 90 mm for the west coast of Norway (4-7° E, 58-63° N) and 35 mm for Svalbard (8-30° E, 76-80° N) (Supplementary Fig. 1).

To evaluate the precipitation extremes simulated by SEAS5, we use a 1x1 km gridded station-based precipitation product for Norway[25]. The data have recently been corrected for underestimation caused by wind-induced under catch and uses more information in the interpolation scheme for data-scarce areas, resulting in higher precipitation in data scarce areas[26]. We upscale this gridded dataset to the same resolution as SEAS5 and extract SON-3DP values for the same spatial domain over 1981-2016. Note, for the Svalbard Archipelago no gridded precipitation dataset is available as a reference dataset. We use ERA5[44] for the global and regional temperature evaluation of SEAS5.

Ensemble member independence testing. The method for independence testing applied in this study is inspired by previous research on potential predictability: the ability of the model to predict itself[32,36]. The potential predictability of a model is calculated by using one of the forecast ensemble members as the observations and the mean of the other ensemble members as the forecast. The correlation between the 'observed' ensemble member and the mean of the other ensemble members is calculated for every ensemble member and this range gives an estimate of the ability of the model to forecast itself. Because this method assesses the correlation between ensemble members, it can be used to find the degree of ensemble members' dependence. In seasonal forecasting, this method is used to identify any predictability in the seasonal prediction system. In contrast, here we seek to demonstrate that there is no potential predictability in the system for the ensemble members to represent independent, unique events.

An illustration of our method to test for independence is shown in Fig. 1. A potential predictability test is performed but instead of correlating an ensemble member to the mean of the other ensemble members, a pairwise correlation test is applied between all ensemble members to robustly assess the individual ensemble member dependence. Indeed, we concatenate the seasons together member by member, even though they do not necessarily originate from the same run. This approach was chosen because the underlying initialization method remains the same for each member over different seasons.

For the 25 ensemble members, there are 300 distinct pairings in the correlation matrix for each of the four lead times being analysed (may-August). We calculate the spearman ρ statistics on the standardized SON-3DP anomalies (deviation from mean divided by the standard deviation) for each distinct pair. From the 300 ρ values for each lead time, boxplot statistics are calculated: the whiskers, the interquartile range and the median. When testing for significance of the 300 ρ values, care must be taken not to falsely detect significant correlations because of the large number of tests. For example, with a confidence interval of 5%, 15 out of the 300 correlations would be expected to be significant by chance alone. To avoid these problems, a permutation test is performed. The dataset, which previously consisted of 25 timeseries (members) of 35 datapoints (years) for four initializations months (lead times), is resampled into 100 timeseries of 35 datapoints, with datapoints randomly picked from all members, years and lead times to remove potential correlations. This randomized dataset is split into four pseudo lead times of 25 timeseries, in order to calculate the boxplot statistics from the same amount of correlation coefficients (300) as before. The data are resampled 1000 times (without replacement), resulting in 4000 boxplot statistics (4 pseudo lead times * 1000 resampled series), from which the confidence intervals are calculated based on a 5% significance level (the 2.5 and 97.5 percentiles).

Model stability. The extreme precipitation distribution must be similar over lead times in order to generate the UNSEEN ensemble. We use four initialization months (May-August) forecasting the target autumn season with lead times 2-5 months. For each lead time, 25 ensemble members over 35 years result into an 875-year long dataset and the pooled ensemble into 3500 years. To compare the distributions, we first plot the probability density function for each of the lead times using ggplot2[56]. Secondly, we plot the extreme value distributions, focussing more on the tails of the distribution. We calculate empirical quantiles of the extreme precipitation ensemble without assuming any distribution a priori, to avoid problems regarding statistical modelling of the extremes[10,57]. The quantile (Q) of a distribution is the inverse of the distribution function ($F(x)$):

$$Q(p) = F^{-1}(p) = \inf \{x: F(x) \geq p\}, \qquad 0 < p < 1 \tag{1}$$

Where the return value is associated with the quantile of percentile (p):

$$p = 1 - \frac{1}{\mathrm{T}} \tag{2}$$

With T being the return period. We use the quantile function in R[58] to compute the empirical return values and we refer to Hyndman & Fan[59] for more specifics.

Fidelity of the UNSEEN ensemble for Western Norway. We first evaluate the UNSEEN ensemble and then compare UNSEEN design-levels to observation-based design-levels. As a first assessment of the biases within the SON-3DP UNSEEN ensemble, we use rank histograms. Rank histograms indicate over-dispersion or under-dispersion and over-forecasting or under-forecasting bias[36]. Here, we have 100 members (4 lead times and 25 ensemble members) for each year over 1981-2015. The rank of the observations within the 100 ensembles is calculated for each year and the resulting 35 ranks are plotted as a histogram over the range 1-100. If the observations are mostly in the upper (lower) ranks, this indicates that the observed values are higher (lower) than the forecasted values and therefore the forecasts are under-forecasting (over-forecasting). Similarly, when the observations are mostly in the outer (inner) ranks, this indicates that the observed values show more (less) variability and thus the forecasts are under-dispersed (over-dispersed). We create rank histograms for the raw SON-3DP UNSEEN ensemble, for the anomalies from the mean and for the standardized anomalies, where the anomalies are divided by the standard deviation.

To compare UNSEEN to the observed record in more detail, we apply a bootstrap test presented in previous studies[20,22]. We bootstrap 10,000 timeseries of 35 years with replacement from all ensembles (100 x 35 years) and calculate the mean, standard deviation, skewness and kurtosis for each. We test whether the four distribution statistics derived from the observed precipitation time series over the period 1981-2015 fall within the 95% confidence intervals for the statistics derived from the bootstrapped timeseries.

We then fit the Generalized Extreme Value (GEV) distribution, described by a location ($-\infty < \mu < \infty$), scale ($\sigma > 0$) and shape ($-\infty < \xi < \infty$) parameter[60]:

$$F(x) = \exp\left[-\left(1 + \xi\left(\frac{x-\mu}{\sigma}\right)\right)^{-\frac{1}{\xi}}\right], \qquad \left(1 + \xi\left(\frac{x-\mu}{\sigma}\right)\right) > 0 \tag{3}$$

And we test the sensitivity to using the Gumbel distribution with $\xi = 0$, simplifying the distribution to:

$$F(x) = \exp\left[-exp\left(-\left(\frac{x-\mu}{\sigma}\right)\right)\right], \qquad -\infty < x < \infty \tag{4}$$

The quantiles of the distribution can again be obtained by inverting the distribution:

$$x_p = \begin{cases} \mu - \frac{\sigma}{\xi}\left[1 - \{-log(1-p)\}^{-\xi}\right], & for\ \xi \neq 0 \\ \mu - \sigma \log\{-log(1-p)\} \quad , & for\ \xi = 0 \end{cases} \tag{5}$$

Where the return value x_p corresponds to the return period 1/probability (p). For all statistical model fits in this study (including non-stationary fits described in the next section), we apply Maximum Likelihood Estimation (MLE) to estimate the parameters of the distributions, utilizing the extRemes package[61] in R[58]. The 95% confidence intervals of the distributions are calculated based on the normal approximation, which is the default of the extRemes package.

UNSEEN-trends. In this study, we present the idea of performing trend analysis on seasonal hindcast, as the seasonal hindcasts provide a larger sample than observations and a higher resolution than climate models (see the UNSEEN-trends section for more details). We apply well-established extreme value theory[60,62,63], by allowing the location (μ) and scale (σ) parameters of the

GEV distribution (given in equation 3) to vary linearly with time (t). Because the scale parameter needs to be positive, a log-link function is used:

$$\mu(t) = \mu_0 + \mu_1 t \quad (6)$$

$$\ln \sigma(t) = \phi_0 + \phi_1 t \quad (7)$$

This approach selects one block maximum per year, leading to 35 data points over the years 1981-2015 based on observed records. With UNSEEN-trends, we have 100 times more values for each year and thus increase confidence in the regression analysis (see Fig.4a,b for illustration). As for the stationary method, we use MLE to estimate the parameters of the distributions and the normal approximation to find the 95% confidence intervals of return values. We focus on the changes in the 100-year quantiles, because these are associated with the design-levels mostly used in flood defence[64]. The trend in the 100-year return value is defined as the percentual change between 1981 and 2015:

$$\Delta x_T = 100 * \left(\frac{x_T(\mu_{2015}, \ln \sigma_{2015}, \xi) - x_T(\mu_{1981}, \ln \sigma_{1981}, \xi)}{x_T(\mu_{1981}, \ln \sigma_{1981}, \xi)} \right)$$

Where x_T is defined by equation (5).

The robustness of the trends to experiment decisions like the block size and the regression method can be further investigated but are beyond the scope of this research. For example, 6-month blocks can be selected at the expense of the ensemble size. This will result in 25 realizations, in comparison with 3-month blocks, which contain 100 realizations. A block size of three months (September-November) is chosen in this study. A linear trend in time is assumed in this study. With the large amount of data, more complex regression methods can be explored. The ECMWF SEAS5 seasonal prediction system is used in this study, but other seasonal prediction systems with available hindcasts could also be assessed to test the model sensitivity to return value and trend estimation.

Acknowledgements

We greatly thank A.V. Dyrrdal, J. Sillmann, A. Weisheimer, and the anonymous reviewers for their input that helped improve the paper. T.K. acknowledges support from NERC CENTA Doctoral Training Partnership and funding from both the Norwegian Meteorological Institute and Loughborough University. M.M. acknowledges funding from the TWEX project (grant 255037).

Data and code availability

SEAS5 re-forecast data was accessed through the MARS Catalogue. This catalogue has restricted access, it is available for National meteorological services of ECMWF Member and Co-operating States. Other users can request access here: https://www. ecmwf.int/en/about/contact-us?subject=Gain%20access%20to%20archive%20data. Alternatively, SEAS5 re-forecast data on 1-degree resolution, as well as ERA5 data, are openly available from the Copernicus Climate Change Service (C3S) Climate DataStore (https://cds.climate.copernicus.eu/). The SeNorge daily total precipitation data are available at https://doi.org/10.5281/zenodo.2082320. The extracted SON3DP UNSEEN ensembles as well as the extracted SON-3DP observations, along with all code to reproduce the analysis in this paper are available on GitHub: https://github.com/timokelder/UNSEEN-trends.

Author contributions

T.K. and M.M. conceived and T.K, M.M, L.J.S., T.M., R.L.W., C.P., P.B. designed the study. T.K. drafted the paper with extensive contributions from L.J.S., T.M., R.L.W., C.P. and M.M.. T.K. analysed the data with input from all authors. M.M. acquired the data. T.K. produced the figures; L.F. produced Supplementary Fig. 6.

Competing interests

The authors declare no competing interests.

Figures

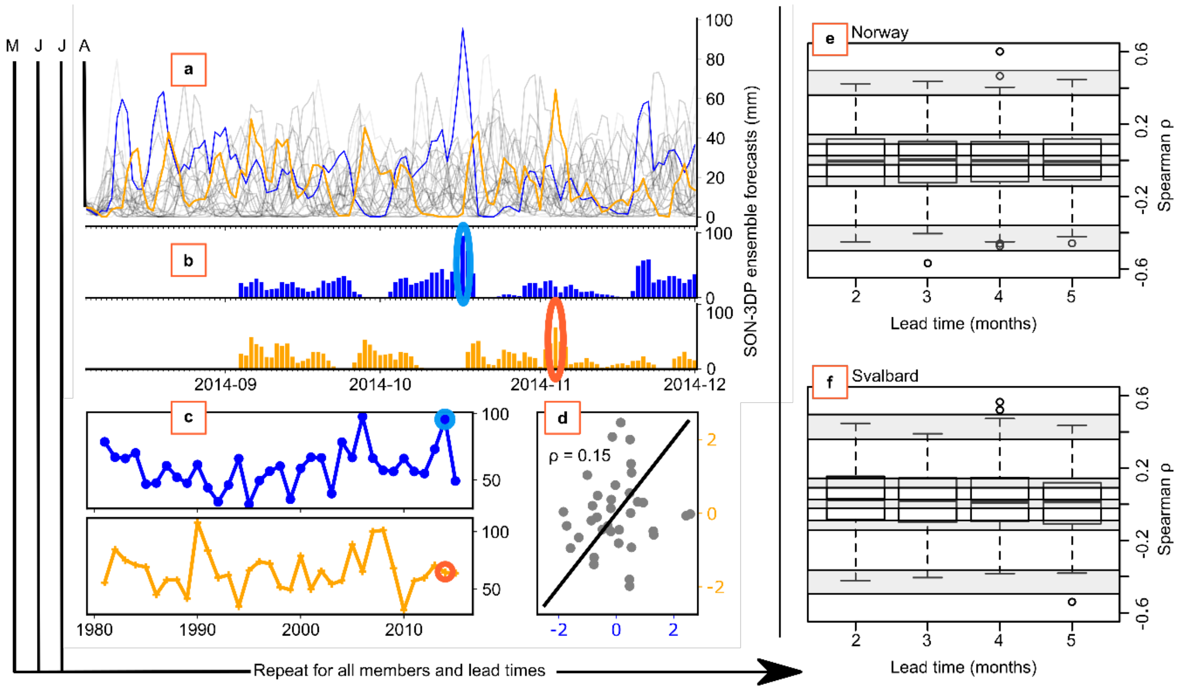

Fig. 1 | A workflow for analysing ensemble member dependence. a, August 2014 initialized 25-member seasonal forecasts of 3-day precipitation time series over the SON forecast horizon. Ensemble members 0 and 1 are shown in blue and orange, respectively. **b,** From the forecast members 0 and 1, the September-November (SON) maximum value for the 2014 season is selected. **c,** A series of the maximum 3-day precipitation values for the SON season for each year in the hindcast record is created for member 0 and member 1. The 2014 maximum, as illustrated in b, is encircled. **d,** The standardized anomaly of the maximum 3-day precipitation series for the two members are correlated. Spearman's *rho* correlation is shown. This process is repeated for the 300 distinct ensemble member pairings for each of the four lead times (May-August). **e,f,** Boxplots of the resulting 300 Spearman's *rho* correlations for each lead time over Norway (**e**) and Svalbard (**f**). Grey shading shows the confidence intervals of the boxplot statistics (whiskers, interquartile range and median), based on a permutation test with 5% significance level.

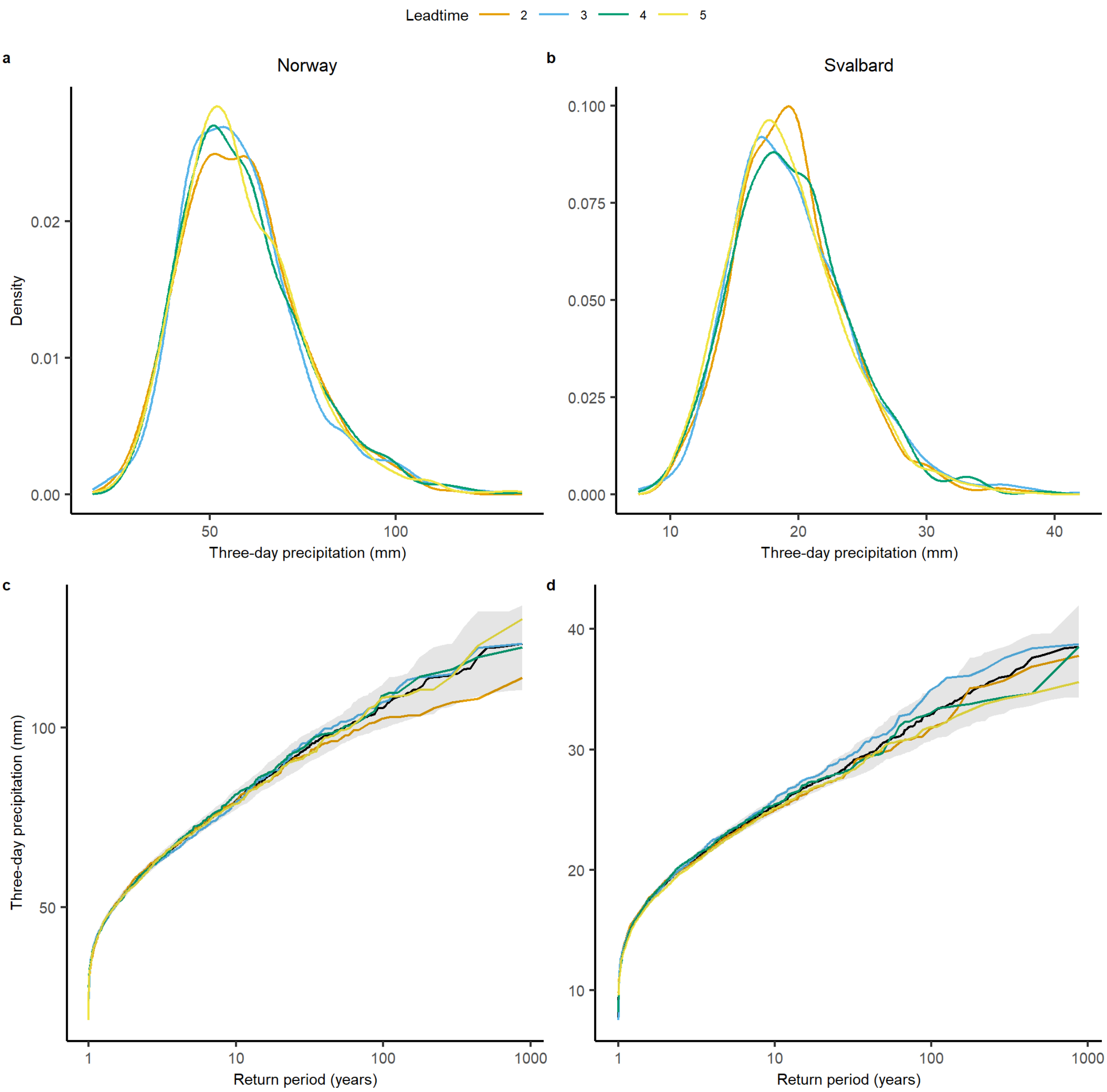

Fig. 2 | SEAS5 model stability of extreme precipitation over Western Norway and Svalbard. The empirical probability density (**a,b**) and extreme value (**c,d**) distribution of SON-3DP for each lead time and for all lead times together (in black), for the West Coast (**a,c**) and Svalbard (**b,d**) domains. Grey shading in **c,d,** illustrates the 95% confidence intervals of the distribution of the pooled lead times, bootstrapped to timeseries of similar length to the individual lead times with n = 10,000.

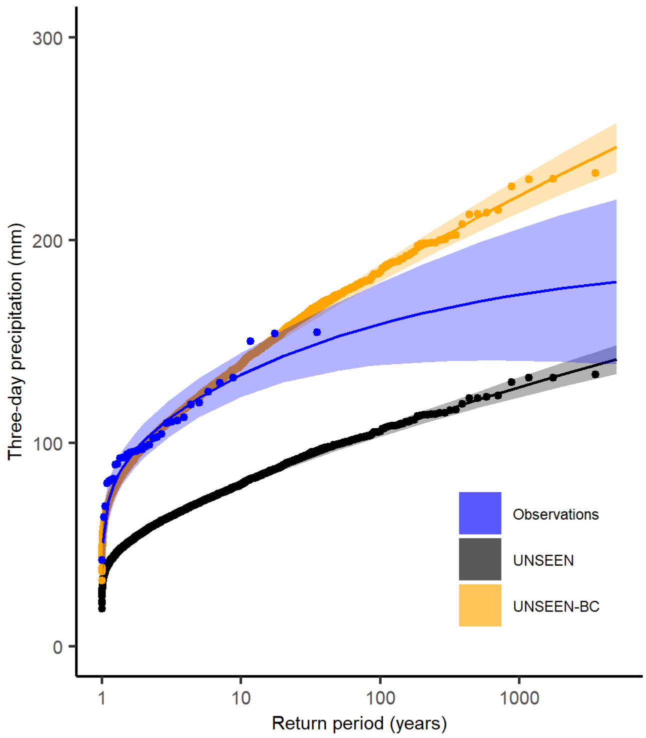

Fig. 3 | The extreme precipitation distribution for UNSEEN and UNSEEN-BC, as compared to the precipitation record over Western Norway. The data points show the SON-3DP events and the solid lines show the GEV fitted to the data, including 95% confidence intervals.

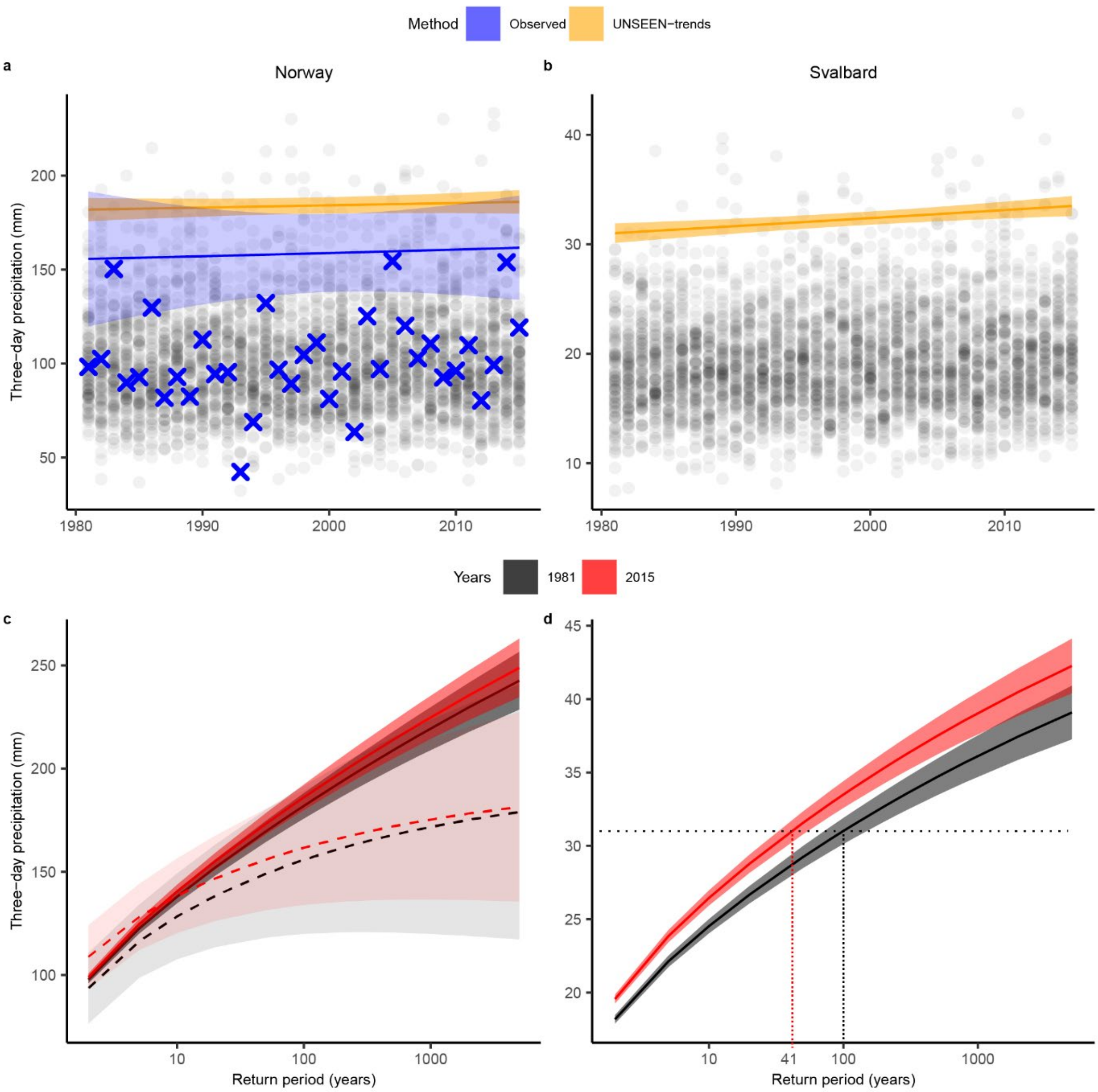

Fig. 4 | UNSEEN-trends in extreme precipitation, as compared to trend analysis based on the precipitation record. a,b, The change in 100-year SON-3DP over 1981-2015 is shown for (**a**) Western Norway and (**b**) Svalbard. The data points show the SON-3DP events in the observed record (blue crosses) and in the UNSEEN-ensemble (black circles). Note, for Svalbard no gridded precipitation record is available and for Norway the bias-corrected UNSEEN-BC is used. **c,d,** In addition to the change in 100-year precipitation, the entire GEV distribution is plotted for the covariates 1981 and 2015 over (**c**) Western Norway and (**d**) Svalbard. Solid lines and dark shading indicate the trend and uncertainty of the UNSEEN-trends approach and dashed lines with light shading (in **c**) indicates the trend and uncertainty range based on observations. In **d**, the magnitude of the event with a return period of 100 years in 1981 is illustrated with black dotted lines and the event of similar magnitude corresponding to a return period of 41 years in 2015 is illustrated with a red dotted line.